Journal of Solid State Chemistry **168,** 52–59 (2002)
doi:10.1006/jssc.2002.9678

Nanocrystalline $Ce_{1-x}Y_xO_{2-x/2}$ ($0 \leq x \leq 0.35$) Oxides via Carbonate Precipitation: Synthesis and Characterization

Ji-Guang Li,[1] Takayasu Ikegami, Yarong Wang, and Toshiyuki Mori

Sintered Materials Research Group, Advanced Materials Laboratory, National Institute for Materials Science, Namiki 1-1, Tsukuba, Ibaraki 305-0044, Japan

Received March 19, 2002; accepted May 30, 2002

A novel carbonate (co)precipitation method, employing nitrates as the starting salts and ammonium carbonate as the precipitant, has been used to synthesize nanocrystalline CeO_2 and $Ce_{1-x}Y_xO_{2-x/2}$ ($x \leq 0.35$) solid-solutions. The resultant powders are characterized by elemental analysis, differential thermal analysis/thermogravimetry (DTA/TG), X-ray diffractometry (XRD), Brunauer–Emmett–Teller (BET) analysis, and high-resolution scanning electron microscopy (HRSEM). Due to the direct formation of carbonate solid-solutions during precipitation, $Ce_{1-x}Y_xO_{2-x/2}$ solid-solution oxides are formed directly during calcination at a very low temperature of $\sim 300^\circ C$ for 2 h. The thus-produced oxide nanopowders are essentially non-agglomerated, as revealed by BET in conjunction with XRD analysis. The solubility of $YO_{1.5}$ in CeO_2 is determined via XRD to be somewhere in the range from 27 to 35 mol%, from which a Y_2O_3-related type-C phase appears in the final product. Y^{3+}-doping promotes the formation of spherical nanoparticles, retards thermal decomposition of the precursors, and suppresses significantly crystallite coarsening of the oxides during calcination. The activation energy for crystallite coarsening increases gradually from 68.7 kJ mol^{-1} for pure CeO_2 to 138.6 kJ mol^{-1} for CeO_2 doped with 35 mol% $YO_{1.5}$. The dopant effects on crystallite coarsening is elaborated from the view point of solid-state chemistry.

Key Words: **(co)precipitation; carbonate; cerium oxide; yttrium oxide; solid solution.**

1. INTRODUCTION

CeO_2 is a fluorite-structured ceramic material which does not show any known crystallographic change from room temperature up to its melting point. When doped with aliovalent cations (alkaline-earth and rare-earth), oxygen vacancies are created in the CeO_2 lattice for charge compensation. CeO_2-based materials are valuable for applications as oxygen buffers in automotive three-way catalysts (TWCs) (1, 2), as promoters for gas-phase oxidation/reduction reactions, and as oxygen-ion conducting electrolytes for solid oxide fuel cells (SOFCs) (3, 4). Among rare-earth (RE)-doped CeO_2, the Y_2O_3/CeO_2 (YDC) system has been the subject of studies due to its relatively high electrical conductivity and the relative abundance of the yttrium element. Unlike CeO_2, Y_2O_3 is a type-C sesquioxide whose structure is a cubic derivative of the fluorite arrangement with a lattice constant double that of the fluorite cell (5).

Besides the traditional ceramic method which requires repeated mechanical mixing and extensive heat treatment, several kinds of wet-chemical approaches have been used to synthesize YDC solid-solutions, including oxalate coprecipitation (6–8), thermal decomposition of trichloroacetates (9), urea-based homogeneous precipitation (10), and hydrothermal treatment (11). The wet-chemically derived YDC oxides generally show finer crystallite sizes and better reactivity than those via solid-state reaction. For the purpose of ceramics fabrication, however, these powders have to be fired at high temperatures of 1400–1600°C to achieve ~99% of the theoretical density. The main problems seem to be the relatively large particle size (submicron to tens of microns), irregular particle shape, and severe agglomeration. Furthermore, previous studies mainly focus on some specific compositions, rarely on systematic studies on the wet-chemical processing and characterization of YDC materials.

The properties of a wet-chemically derived oxide powder is known to heavily depend upon precursor characteristics, exhibiting the existence of some sort of "genetic" relationship. Our previous work on $Y_3Al_5O_{12}$ (12) and $MgAl_2O_4$ (13) showed that carbonate coprecipitation is a facile method to produce multi-cation oxides of good dispersion and excellent reactivity. The synthetic method is expected to be effective for mixed *RE* oxides, as *RE* elements readily

[1]To whom correspondence should be addressed. Fax: +81-298-52-7449. E-mail: li.jiguang@nims.go.jp.

0022-4596/02 $35.00

form carbonate solid-solutions (14), which allows low-temperature formation of the aimed phase. In this work, the carbonate (co)precipitation method, employing nitrates as the starting salts and ammonium carbonate as the precipitant, is used to produce CeO_2 and $Ce_{1-x}Y_xO_{2-x/2}$ ($x \le 0.35$) solid-solutions. In the following sections, we report the synthesis and characterization of these carbonate-derived oxides. The effects of yttrium concentration on powder properties are also discussed.

2. EXPERIMENTAL PROCEDURE

2.1. Powder Synthesis

Precursors for $Ce_{1-x}Y_xO_{2-x/2}$ oxides ($x = 0$, 0.025, 0.05, 0.10, 0.15, 0.20, 0.27, and 0.35, respectively) are produced via precipitation using ammonium carbonate ($(NH_4)_2CO_3$, ultrahigh purity) as the precipitant. These oxides will later be referred to as 0-35YDC for convenience. The starting salts are cerium and yttrium nitrate hexahydrates ($RE(NO_3)_3 \cdot 6H_2O$, RE = Ce and Y) with a purity of at least 99.99% (Kanto Chemical Co. Inc., Tokyo, Japan). All the chemicals are used as received without further purification.

The stock solutions were made by dissolving the cerium and yttrium salts into distilled water. To make sure that Ce^{3+} and Y^{3+} cations would be mixed at the predetermined molar ratios, cation contents of the mixed solutions were assayed by the inductively coupled plasma (ICP) spectrophotometric technique and further adjusted. The final concentration of each stock solution was 0.15 M for Ce^{3+} (excluding Y^{3+} cations). Aqueous solutions of ammonium carbonate with a concentration of 1.5 M were used as the precipitant.

In a typical synthetic procedure, 300 cm^3 of the mixed salt solution was dripped at a speed of 5 cm^3 min^{-1} into 300 cm^3 of the precipitant solution kept at 70°C under mild stirring. The resultant suspension, after homogenizing for 1 h, was filtered via suction filtration. The precipitate cake was washed repeatedly with distilled water and finally rinsed with anhydrous alcohol (except those for chemical analysis) before drying at room temperature with flowing nitrogen gas. The dried precursor was lightly crushed with a zirconia mortar and pestle and then calcined under flowing oxygen gas (50 cm^3 min^{-1}) at various temperatures for 2 h to yield oxide powders.

2.2. Powder Characterization

Composition of the precursor was determined via elemental analysis. Cation contents were determined by the ICP method with an accuracy of 0.01 wt%; carbon (from carbonate anions) content was assayed on a simultaneous carbon/sulfur determinator with a detection limit of 0.01 wt% (Model CS-444LS, LECO, St. Joseph, MI, USA); NH_4^+ content was determined by the distillation-titrimetric method with an experimental error of ± 0.1 wt%; NO_3^- content was analyzed by the spectrophotometric method on a Ubest-35 spectrophotometer (Japan Spectroscopic Co. Ltd, Tokyo, Japan) with an accuracy of 0.01 wt%.

Differential thermal analysis/thermogravimetry (DTA/TG) of the dried precursors was made on a TG-DTA analyzer (Thermo Plus TG8120, Rigaku, Tokyo, Japan) in flowing air with a heating rate of 10°C min^{-1}. The sample crucible is platinum, and the reference material is alpha-alumina.

Phase identification was performed via X-ray diffractometry (XRD) on a Philips PW1800 X-ray diffractometer (Philips Research Laboratories, The Netherlands) operating at 40 kV/50 mA using nickel-filtered Cu$K\alpha$ radiation in the range of $2\theta = 20-100°$ with a scanning speed of 1.5° 2θ min^{-1}. Lattice parameters of the YDC solid-solutions were determined by fitting the observed reflections with a least-squares refinement program. Crystallite sizes (D_{XRD}) of the calcined powders were calculated by the X-ray line broadening technique performed on the (422) diffraction of CeO_2 lattice using a computer software (APD 1800, Philips Research Laboratories) from the Scherrer equation [15]:

$$D_{XRD} = K\lambda/\beta \cos\theta, \quad [1]$$

where θ is the Bragg angle of diffraction lines, K is a shape factor ($K = 0.9$ in this work), λ is the wavelength of incident X-rays (0.15406 nm), and β is the corrected half-width given by

$$\beta^2 = \beta_m^2 - \beta_s^2, \quad [2]$$

where β_m is the measured half-width and β_s is the half-width of a standard CeO_2 sample with a known crystallite size of larger than 150 nm.

Specific surface area of the calcined powders, S_{BET}, was measured by the Brunauer–Emmett–Teller (BET) method on an automatic surface area analyzer (Model 4201, Beta Scientific Corporation, Albertson, NY, USA) via nitrogen chemisorption at 77 K. The single point BET method was used to determine the surface area. Prior to analysis, the powders were degassed at 125°C for more than 2 h to eliminate the absorbed moisture. The specific surface area was converted into particle/crystallite size according to the following equation assuming that the particles are closed spheres with smooth surface and uniform size:

$$D_{BET} = 6 \times 10^3/(d_{th} S_{BET}), \quad [3]$$

where d_{th} is the theoretical density of the material (g cm^{-3}), D_{BET} (nm) is the average particle/crystallite size, and S_{BET} is the specific surface area expressed in m^2 g^{-1}. Assuming that the dopants are homogeneously distributed in the CeO_2 structure and occupy the Ce^{4+} sites to form a solid solution of $Ce_{1-x}Y_xO_{2-x/2}$, the d_{th} values can be calculated

according to

$$d_{th} = 4[(1-x)M_{Ce} + xM_Y + (2-x/2)M_O]/a^3 N_A, \quad [4]$$

where a is the lattice constant of the YDC material at room temperature, N_A is the Avogadro constant, and M refers to the atomic weight.

Particle morphologies of the YDC powders were observed via high-resolution scanning electron microscopy (HRSEM) (Model S-5000, Hitachi, Tokyo, Japan). Samples were ultrasonically dispersed in ethanol, and the suspensions were then spread on silicon plates. Osmium coating was performed before observation for better conductivity.

3. RESULTS AND DISCUSSION

3.1. Synthesis and Composition of the Precursor

Yttrium doping was found to have appreciable effects on precursor properties. The precursors for 0-10YDC are very easy to wash via suction filtration and are very porous and voluminous after drying. The 15-35YDC precursors, however, are relatively difficult to wash, and the dried precipitate cakes show much smaller volumes. This phenomena suggests that chemical composition or particle morphology of the precursor varies with the doping level.

Chemical analysis confirmed that, within the accuracy of the analysis method (0.01 wt%), the precursors possess the predetermined stoichiometry. NO_3^- is non-precipitating here and its content in the precursor is below the detection limit (0.01 wt%). The precursor for pure CeO_2 (0YDC) was determined via elemental analysis to be a cerous double carbonate with an approximate composition of $(NH_4)_{0.25}Ce(CO_3)_{1.625} \cdot H_2O$. The yttrium-doped precursors, however, assume an approximate formula of $(NH_4)_{0.20}Ce_{(1-x)}Y_x(CO_3)_{1.60} \cdot 1.6H_2O$, regardless of the dopant concentration. To understand the precipitation behavior of Y^{3+} cations, a precursor for pure Y_2O_3 was prepared separately from a 0.15 mol dm^{-3} nitrate solution under conditions identical to those described in the experimental section, and its composition was found to be $(NH_4)Y(CO_3)_2 \cdot 1.3H_2O$. Obviously, the doped precursors are not a simple combination of $(NH_4)_{0.25}Ce(CO_3)_{1.625} \cdot H_2O$ and $(NH_4)Y(CO_3)_2 \cdot 1.3H_2O$ according to their respective Ce/Y molar ratios.

The ammonium double carbonates obtained in this work are analogous to the sodium *RE* carbonates ($NaLn(CO_3)_2 \cdot xH_2O$, *Ln* = lanthanoids and Y) (16) precipitated with sodium carbonate from nitrate solutions. Carbonate double salts of *RE* elements were reported (17) to follow a general formula of $M_x[RE(CO_3)_{1.5+x/2}] \cdot nH_2O$ ($M = NH_4^+$, Na^+, K^+, and Rb^+; *RE* = La–Lu and Y), where the x value may vary up to 6, depending upon the processing conditions. The precursors produced in this work show x values much lower than 6 (even smaller than unity except for the Y_2O_3 precursor), which may indicate that the *RE* cations have not been fully coordinated during precipitation and/or the precursors have undergone partial decomposition during drying. Unlike their alkali counterparts, ammonium double carbonates show lower stability and may lose ammonia and carbon dioxide readily (18).

3.2. Results of DTA/TG Analysis

The thermal decomposition behaviors of *RE* normal carbonates have been studied systematically and are well documented (19, 20). It was reported that cerous carbonate hydrate ($Ce_2(CO_3)_3 \cdot 8H_2O$) decomposes into ceria via dioxymonocarbonate ($Ce_2O_2CO_3$) intermediate while yttrium carbonate hydrate ($Y_2(CO_3)_3 \cdot 3H_2O$) via two intermediate compositions: oxydicarbonate ($Y_2O(CO_3)_2$) and dioxymonocarbonate ($Y_2O_2CO_3$).

Figure 1 shows DTA/TG curves of the as-dried precursors. The results obtained on 2.5YDC, 5YDC, 20YDC and 27YDC precursors are omitted to maintain clarity of the figure. It should be noted that the 2.5YDC and 5YDC samples are intermediate in decomposition behavior between 0YDC and 10YDC, while 20YDC and

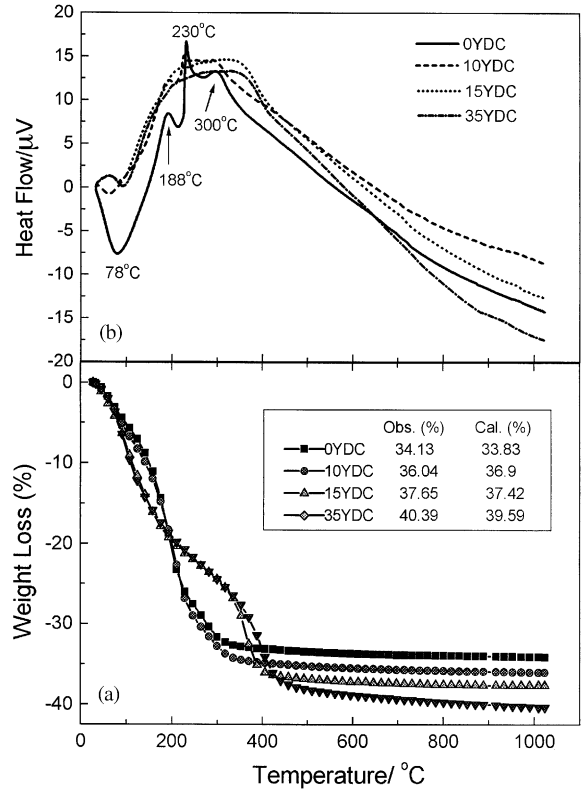

FIG. 1. Simultaneous DTA/TG curves of the as-dried precursors with (a) TG and (b) DTA. The data were taken in air at a heating rate of 10°C min^{-1}.

27YDC are intermediate between 15YDC and 35YDC. Furthermore, these four omitted samples follow the general trend concerning the effect of doping level on thermal decomposition.

It can be seen from Fig. 1a that the 0YDC precursor decomposes into oxide through three distinct stages, with the first one corresponding to the release of ammonia and molecular water to form $Ce(CO_3)_{1.5}$, the second one corresponding to the partial decomposition of $Ce(CO_3)_{1.5}$ to generate $Ce_2O_2CO_3$, and the third one corresponding to the decomposition of $Ce_2O_2CO_3$ to yield CeO_2. The calculated weight losses for the first two stages (11.53% and 28.45%, respectively) agree well with those revealed by TG analysis (11.04% at 158°C and 28.89% at 264°C, respectively). The final weight loss (34.13%) revealed by TG is also in excellent agreement with that (33.83%) calculated from the chemical formula of the precursor, noticing the oxidation of Ce^{3+} cations to Ce^{4+} during the last stage of decomposition. In accordance with TG analysis, the DTA curve (Fig. 1b) shows several thermal events corresponding to the decomposition process. The large endothermic peak centered at ~78°C was caused by the first-stage decomposition. The second stage starts from ~188°C, and the exothermic peak at ~230°C may be caused by the crystallization of $Ce_2O_2CO_3$ intermediate. The endotherm corresponding to the third stage may have been overshadowed by the exotherm peaked at ~230°C and was not clearly identified on the DTA curve. The broad exotherm centered at ~300°C is likely formed by the oxidation of Ce^{3+} to Ce^{4+} and the crystallization of CeO_2.

Doping level has appreciable effects on the thermal decomposition process: the precursor with a higher yttrium content shows weaker thermal events on the DTA curve (Fig. 1b) while requires a higher decomposition temperature (Fig. 1a). Decomposition is nearly complete for 0YDC at ~300°C, while ~450°C is necessary for 35YDC. It was also noticed that the precursors doped up to 10 mol% Y^{3+} show similar TG curves to the 0YDC precursor while those doped with 15 mol% Y^{3+} or above are similar to the yttrium normal carbonate ($Y_2(CO_3)_3 \cdot nH_2O$) in thermal behavior (20). This phenomena indicates that thermal decomposition of the precursor is mainly dominated by the cerium component at lower doping levels ($\le$10 mol%) but governed by the yttrium component at higher doping levels ($\ge$15 mol%).

3.3. Results of XRD Analysis

Figure 2 shows XRD patterns of the as-dried precursors. The precursors for pure CeO_2 and the yttrium-doped ones exhibit low crystallinity, making it difficult to perform phase identification. The precursor for Y_2O_3 is well crystallized, but the diffraction peaks cannot be indexed by comparing with the data files of known yttrium

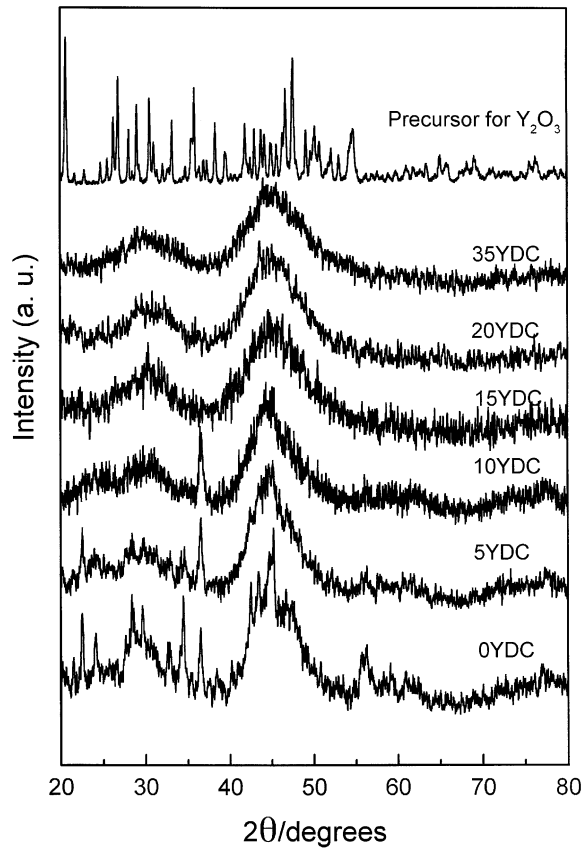

FIG. 2. XRD patterns of the as-dried precursors. Notice the gradually decreased crystallinity with an increase in the dopant concentration.

compounds. The doped precursors, at any doping level, show no reflections corresponding to the Y_2O_3 precursor, and their crystallinity decreases gradually with increasing the doping level. The above observations may suggest that solid solutions of the Ce/Y system have been formed directly during precipitation.

We have made a systematic study on the phase evolution of the YDC precursors upon calcination. Each precursor was treated at the selected temperatures (up to 1400°C) for 2 h under flowing oxygen gas and then subjected to XRD analysis after cooling down. It was observed that all the precursors, regardless of the dopant concentration, begin to crystallize into the fluorite-structured oxides from ~300°C. The 0YDC sample (Fig. 3) has exhibited nearly all the characteristic reflections corresponding to the fluorite-structured CeO_2 (JCPDS 34-394) at 300°C, and the peaks grow narrower and sharper at higher temperatures, indicating crystallite growth. At the same calcination temperature of 300°C, the doped samples show successively lower crystallinity at a higher doping level, mainly due to incomplete decomposition. This observation is in accordance with the results of TG analysis (Fig. 1a). The 0-27YDC samples show no other crystalline phase except the fluorite-type solid-solution at any calcination

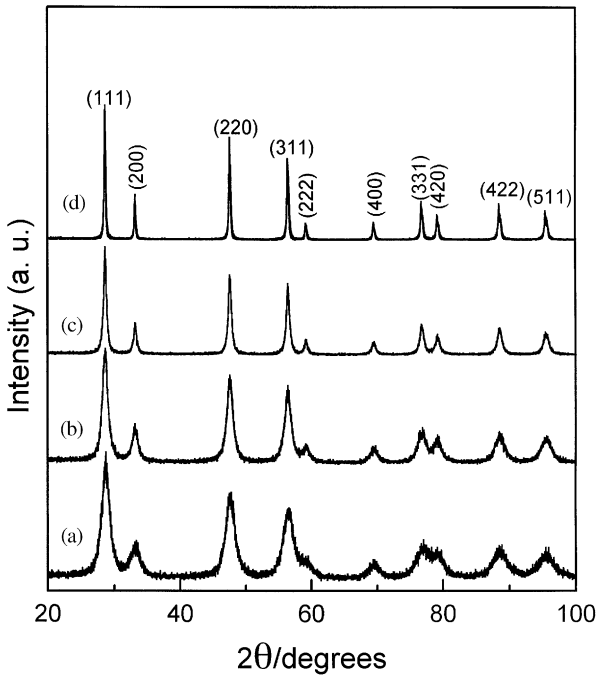

FIG. 3. XRD patterns of the 0YDC (CeO_2) powders calcined for 2 h at (a) 300°C, (b) 500°C, (c) 700°C, and (d) 1000°C.

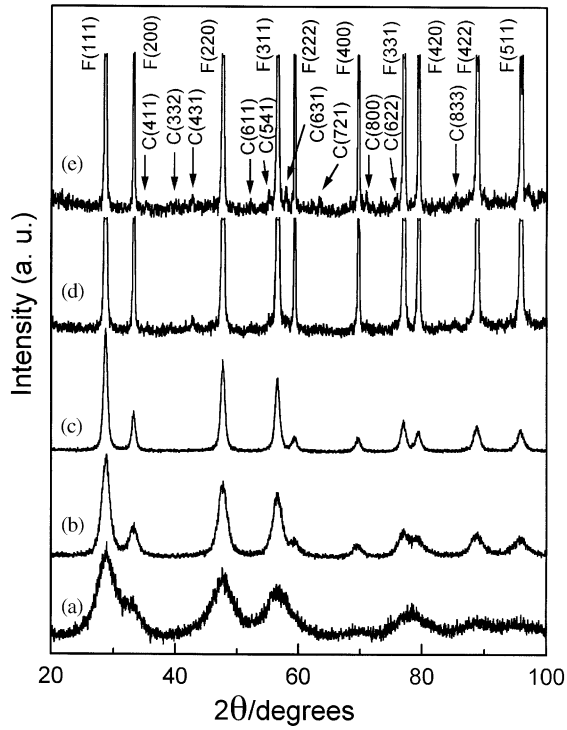

FIG. 4. XRD Patterns of the 35YDC powders calcined for 2 h at (a) 300°C, (b) 500°C, (c) 700°C, (d) 1000°C, and (e) 1400°C. Some diffraction peaks in (d) and (e) were truncated to envision the trace type-C phase. F: fluorite-type solid-solution; C: type-C phase.

temperature up to 1400°C. The 35YDC powder (Fig. 4), however, is diphasic after calcination at 500°C: a trace amount of type-C phase (21) appeared along with the fluorite-type solid-solution. Both phases show sharper reflections at a higher calcination temperature, but the type-C phase does not vanish even after prolonged heating at 1400°C. Thus, one may conclude that the solubility limit of $YO_{1.5}$ in CeO_2 is around 35 mol%.

The lattice constants of the 0-35YDC oxides calcined at 700°C have been determined using a computer program based on the Rietveld method. Yttrium doping induced a gradual contraction in the unit cell. The lattice parameters as well as some other properties of the 0-35YDC oxides are summarized in Table 1. The crystallite sizes determined via XRD and BET are in good agreements, indicating that the two methods have essentially detected the same entities and the powders are essentially non-agglomerated. (In this work, crystallite sizes of the oxides were estimated via XRD without considering the presence of lattice strains. Quantitative information on the size/strain of crystalline powders can be obtained via more sophisticated analysis in XRD from the so-called Hall equation.)

3.4. Crystallite Coarsening Behavior of the $Ce_{1-x}Y_xO_{2-x/2}$ Materials

The low formation temperature (~300°C) permits one to "tailor" the crystallite sizes of pure and yttrium-doped CeO_2 oxides in a wider range of temperatures. The crystallite coarsening behaviors of these carbonate-derived oxides have been monitored up to 900°C, and the results are presented in Fig. 5. It can be seen that yttrium doping suppresses crystallite growth, and the material of a higher doping level shows a smaller crystallite size at the same calcination temperature. The exponential dependence of crystallite size on the calcination temperature indicates that the coarsening process is diffusion related.

TABLE 1
Some Physical Properties of the $Ce_{1-x}Y_xO_{2-x/2}$ ($0 \le x \le 0.35$) Powders Calcined at 700°C for 2 h

Sample I.D.	Crystallite size (nm)		Lattice constant (nm)	ρ_{th} (g cm^{-3})
	D_{XRD}	D_{BET}		
0YDC	20.65	24.10	0.54131	7.210
2.5YDC	19.39	21.12	0.54125	7.151
5.0YDC	18.42	19.94	0.54118	7.091
10YDC	17.05	19.23	0.54099	6.975
15YDC	15.72	16.02	0.54082	6.857
20YDC	12.29	13.15	0.54065	6.739
27YDC	11.34	13.45	0.54027	6.578
35YDC	8.89	9.21	0.53993[a]	6.391

[a] Two-phase sample, determined from the fluorite phase.

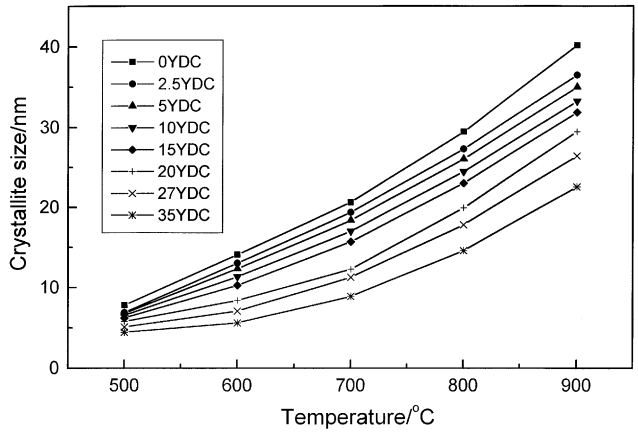

FIG. 5. The crystallite sizes of 0-35YDC oxides, as a function of the calcination temperature.

Crystallite growth generally follows the empirical equation (22):

$$D^n - D_0^n = k(t - t_0), \qquad [5]$$

where D is the average crystallite size at time t, D_0 the average crystallite size at time t_0, n an exponent which, depending upon various kinetic aspects involved in the coarsening process, can assume an integer value ranging from 1 to 4, and k a temperature-dependent rate parameter. For a thermally activated growth process, $k = A\exp(-E_a/RT)$, where A is a constant, R is the gas constant, T is the absolute temperature, and E_a denotes the apparent activation energy for crystallite growth. Taking D_0 as the crystallite size at 500°C, we observed that the coarsening of pure CeO_2 powder follows the parabolic law ($n = 2$) while the doped ones follow the cubic law ($n = 3$). Figure 6 shows the temperature dependence of crystallite size on a log–log plot, with activation energies indicated in the figure. It clearly shows that the material of a higher yttrium content exhibits a higher activation energy upon coarsening.

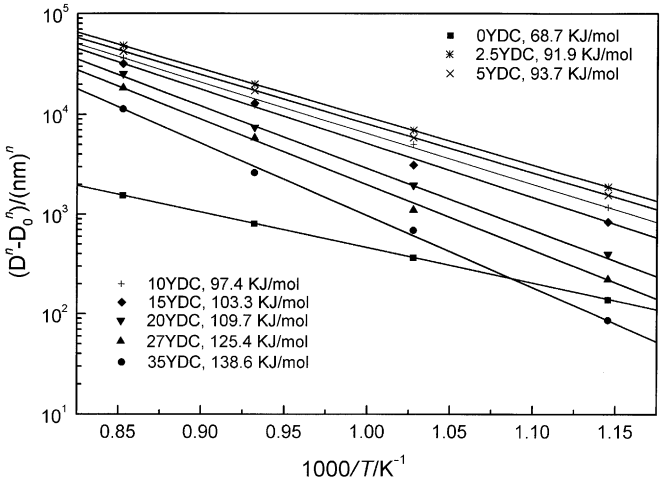

FIG. 6. Crystallite size against reciprocal temperature on a log–log plot, with apparent activation energies indicated. Notice that n is 2 for 0YDC while equals 3 for the rest.

The apparent activation energy for pure CeO_2 found in this work (68.7 kJ mol^{-1}) agrees well with that reported for the CeO_2 powder derived from thermal decomposition of ammonium ceric nitrate (65 kJ mol^{-1}) (23), but is much different from the values reported for the CeO_2 produced via thermal decomposition of cerous oxalate (125 kJ mol^{-1}) (23), cerous nitrate (46 and 203 kJ mol^{-1}) (23), and hydrated ceria oxides (157 and 231 kJ mol^{-1}) (24). This phenomena indicates that the crystallite coarsening behavior and mechanism are precursor dependent. Crystallite coarsening is a process of mass transportation which is closely related with the defects in the crystal structure. For the YDC materials in this study, oxygen diffusion is expected to be much faster than cation diffusion, and the latter is always the rate-controlling factor for crystallite coarsening. The low activation energy of CeO_2 (68.7 kJ mol^{-1}) found in this study implies that cation-transport is likely surface-diffusion related. Indeed, CeO_2 always possesses intrinsic oxygen vacancies due to its high susceptibility to reduction, preferentially on surfaces (25):

$$O_o \rightarrow V_o^{\cdot\cdot} + 2e' + \tfrac{1}{2}O_2. \qquad [6]$$

The changed coarsening mechanism and the gradually increased activation energy by yttrium doping may be explained from the following two aspects:

(1) Yttrium doping introduces extrinsic oxygen vacancies into the crystal interior of CeO_2, and the defect reaction of which can be expressed as:

$$Y_2O_3 \xrightarrow{CeO_2} 2Y'_{ce} + V_o^{\cdot\cdot} + 3O_o^x, \qquad [7]$$

where the symbols have their usual meanings in the Kroger–Vink notations. That is, every two Y^{3+} cations create one $V_o^{\cdot\cdot}$ for charge compensation. As extrinsic oxygen vacancies are introduced into the crystallite interior, cation transport via crystallite-boundary and/or bulk diffusion must have been gradually involved in the coarsening process;

(2) In the dilute doping range (up to $\sim$8.0 mol% Y^{3+}) (26), the Y'_{ce} and $V_o^{\cdot\cdot}$ can be regarded as non-interacting and are in a free state. At higher doping levels, however, the clustering of Y^{3+} cations and the formation of ($Y'_{ce}-V_o^{\cdot\cdot}$) pairs (defect aggregation) are expected considering static electrical attraction. Besides, the difference in the sizes of Y^{3+} and Ce^{4+} cations (considering 8-fold coordination, 0.1019 nm for Y^{3+} and 0.097 nm for Ce^{4+}) (27) is expected to cause local distortion in the crystal lattice. The strain energy caused by lattice distortion and the defect aggregation may slow down the mobility of cations, causing slower coarsening rates of the crystallites.

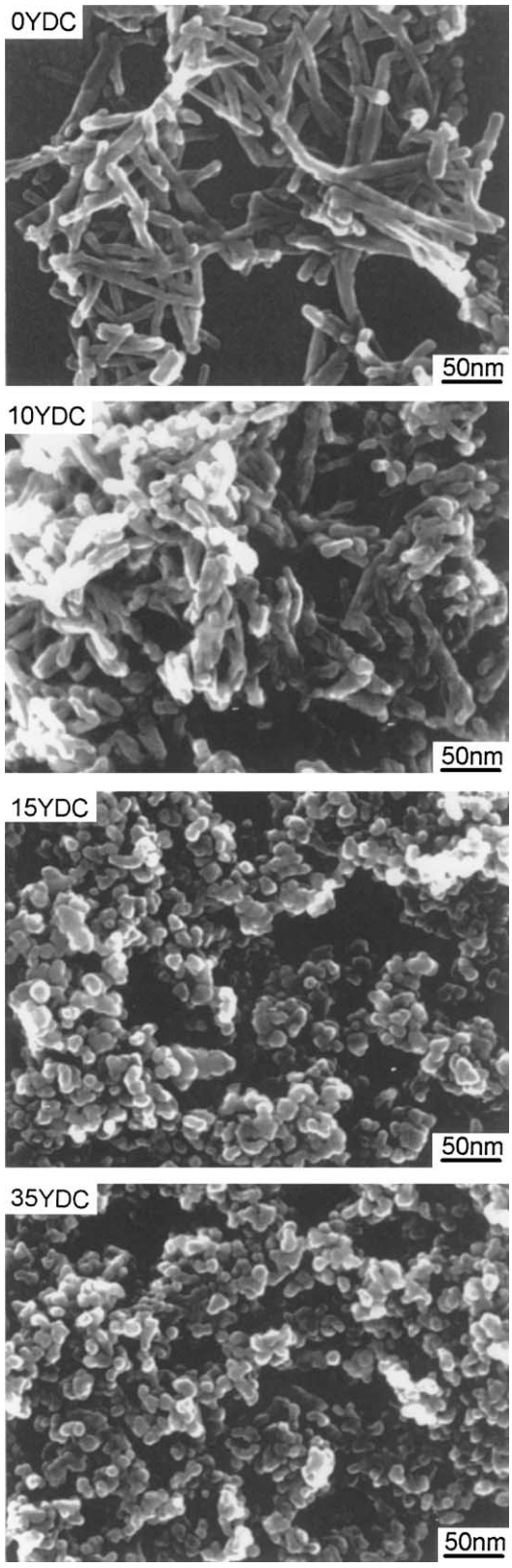

FIG. 7. HRSEM micrographs showing particle morphologies of the precursors. Notice the gradual change in particle morphology with yttrium doping.

3.5. Particle Morphologies of the Precursors and the Calcined Powders

Observations via high-resolution scanning electron microscopy (HRSEM) revealed that yttrium doping affects significantly particle morphology of the precursor, as shown in Fig. 7 for some typical compositions. The 0-10YDC precursors are mainly composed of nanorods (up to $\sim$15 nm in diameter and 150 nm in length), whose aspect ratios decrease gradually with increasing the doping level. The 15–35YDC precursors only contain well-dispersed spherical particles sized up to $\sim$15 nm.The gradual morphological change with an increase in the dopant concentration may be ascribed to the direct formation of carbonate solid-solutions during precursor preparation and the doping effects of Y^{3+} cations.

The variance in particle morphology with yttrium doping explains well the phenomena observed during precursor preparation: The ease of washing and the fluffy nature of 0-10YDC precursors are mainly due to the bridging of rod-like particles, which makes the precipitate cakes porous. The spherical particles in 15-35YDC, on the other hand, are expected to undergo close packing during suction filtration, making the precursors difficult to wash and show smaller volumes upon drying.

Calcination affects particle morphologies of the 0-10YDC materials. At temperatures below 700°C, rod-like particles are predominant in the resultant oxides, though their aspect ratios decrease gradually with an increase in the calcination temperature. At 700°C, the nanorods in the 0-10YDC precursors have been almost completely collapsed into rounded particles measuring less than 30 nm (Figs. 8a and 8b), a morphology more suitable to consolidation and ceramic fabrication. For 15–35YDC materials, however, little change in particle morphology is observed by calcination up to 700°C (Figs. 8c and 8d). At even higher temperatures, the particles of all the YDC materials become faceted due to the increased crystallinity, though the pictures are not shown here.

4. CONCLUSIONS

Carbonate (co)precipitation, employing nitrates as the starting salts and ammonium carbonate as the precipitant, is a facile and effective method to synthesize nanocrystalline CeO_2 and Y^{3+}-substituted CeO_2 solid-solutions. The precursors produced in this work are ammonium rare-earth double carbonates, which decompose into oxides up to $\sim$450°C, depending upon the dopant concentration. YDC solid-solutions are formed directly during calcination at a very low temperature of $\sim$300°C due to the direct formation of carbonate solid-solutions during precipitation and hence the intimate mixing of Ce^{4+} and Y^{3+} cations in the precursors. The solubility of $YO_{1.5}$ in CeO_2 was

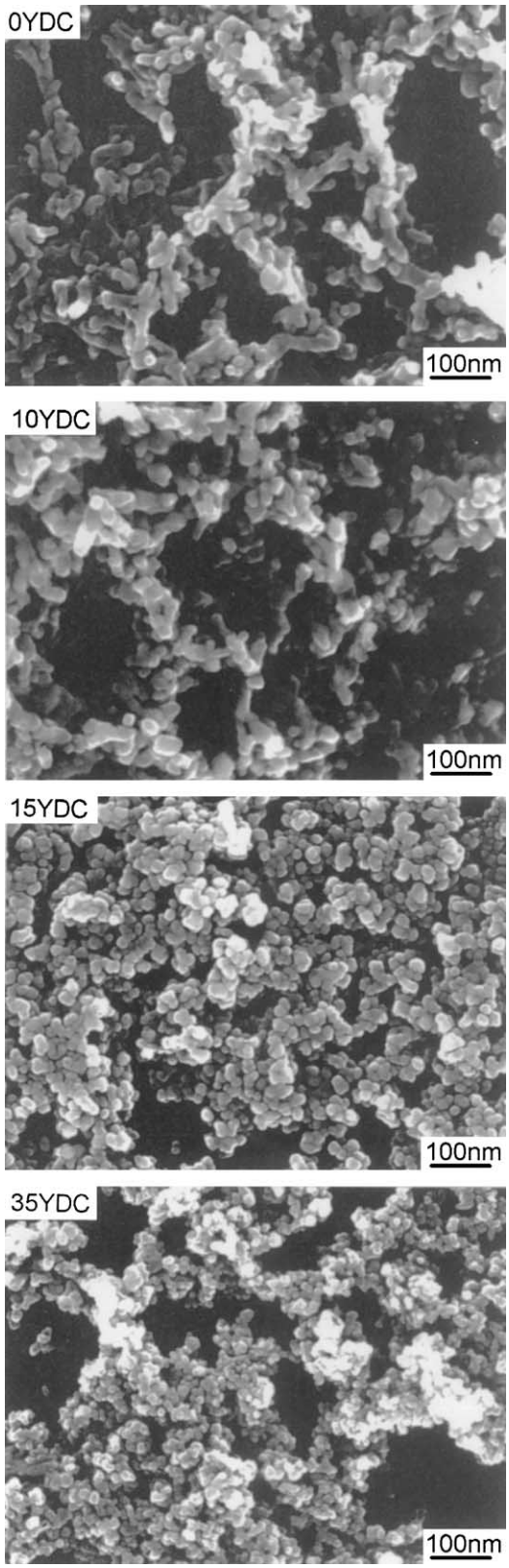

FIG. 8. HRSEM micrographs showing particle morphologies of the powders calcined at 700°C for 2 h. Notice the collapse of rod-like particles in 0-10YDC precursors.

determined via XRD to be between 27 and 35 mol%, after which a Y_2O_3-related type-C phase appears in the final product. Y^{3+} doping promotes the formation of spherical nanoparticles, retards the thermal decomposition of the precursor, and suppresses significantly crystallite coarsening of the solid solution oxides.

REFERENCES

1. H. C. Yao and Y. F. Yao, *J. Catal.* **86,** 254–265 (1984).
2. S. Lemaux, A. Bensaddik, A. M. J. Van der Eerden, J. H. Bitter, and D. C. Koningsberg, *J. Phys. Chem. B***105,** 4810–4815 (2001).
3. H. Yahiro, T. Ohuchi, K. Eguchi, and H. Arai, *J. Mater. Sci.* **23,** 1036–1041 (1988).
4. H. Yahiro, K. Eguchi, and H. Arai, *Solid State Ionics* **36,** 71–75 (1989).
5. M. G. Paton and E. N. Maslen, *Acta Crystallogr.* **19,** 307–310 (1965).
6. P. Duran, C. Moure, and J. R. Jurado, *J. Mater. Sci.* **29,** 1940–1948 (1994).
7. J. V. Hertle, T. Horita, T. Kawada, N. Sakai, H. Yokokawa, and M. Dokiya, *Ceram. Int.* **24,** 229–241 (1998).
8. Higashi, K. Sonoda, H. Ono, S. Sameshita, and Y. Hirata, *J. Mater. Res.* **14**, 957–967 (1999).
9. A. L. Dragoo and L. P. Domingues, *J. Am. Ceram. Soc.* **65,** 253–259 (1982).
10. B. Aiken, W. P. Hsu, and E. Matijevic, *J. Am. Ceram. Soc.* **71,** 845–853 (1988).
11. K. Yamashita, K. V. Ramanujachary, and M. Greenblatt, *Solid State Ionics* **81,** 53–60 (1995)
12. J.-G. Li, T. Ikegami, J.-H. Lee, and T. Mori, *J. Mater. Res.* **15,** 1514–1523 (2000).
13. J.-G. Li, T. Ikegami, J.-H. Lee, and T. Mori, *J. Am. Ceram. Soc.* **11,** 2866–2868 (2000).
14. H. Wada and S. Kinoshita, *Bull. Chem. Soc. Jpn.* **52,** 428–432 (1979).
15. P. Klug and L. E. Alexander, "Diffraction Procedures for Polycrystalline and Amorphous Materials." Wiley, New York, 1954.
16. V. H. Schweer and H. Z. Seidel, *Anorg. Allg. Chem.* **477,** 196–204 (1981).
17. D. I. Ryabchikov and E. A. Terentyeva, *in* "Progress in the Science and Technology of the Rare Earth I" (L. Eyring, Ed.), p. 139. Pergamon Press, New York, 1964.
18. E. Erdos, H. Altorfer, and J. Witt, *J. Appl. Cryst.* **12,** 611–612 (1979).
19. E. L. Head and C. E. Holly Jr., *in* "Rare Earth Research II" (K. S. Vorres, Ed.), p. 51. Gordon and Breach, London, 1964.
20. E. L. Head and C. E. Holly Jr., *in* "Rare Earth Research III" (L. Eyring, Ed.), p. 707. Gordon and Breach, London, 1965.
21. N. Gabbitas, J. G. Thompson, R. L. Withers, and A. D. Rae, *J. Solid State Chem.* **115,** 23–26 (1995).
22. R. J. Brook, *in* "Ceramic Fabrication Processes" (F. F. Y. Wang, Ed.), p. 235. Academic Press, New York, 1976.
23. K. A. El-Adham and A. M. M. Gadalla, *Interceram* **3,** 223–330 (1977).
24. N. Audebrand, J. P. Auffredic, and D. Louer, *Chem. Mater.* **12,** 1791–1799 (2000).
25. T. X. T. Sayle, S. C. Parker, and C. R. A. Catlow, *Surf. Sci.* **316,** 329–336 (1994).
26. D. Y. Wang, D. S. Park, J. Griffith, and A. S. Nowick, *Sold State Ionics* **2,** 95-105 (1981).
27. R. D. Shannon, *Acta Crystallogr. A* **32,** 751–767 (1976).